Depth-Sensitive Cerebral Blood Flow and Low-Frequency Oscillations for Consciousness Assessment Using Time-Domain Diffuse Correlation Spectroscopy

Sahar Sabaghian[1], Chien-Sing Poon[2], Carsi Kim[1], Christopher H Moore[1], Irfaan Dar[1], Timothy M. Rambo[3], Aaron J. Miller[3], Sujith Swarna[4], Noah Lubin[4], Sima Mofakkam[4], Charles Mikell[4], Jingxing Wang[4], Brandon Foreman[5], and Ulas Sunar[1*]

[1]Dept of Biomedical Engineering, Stony Brook University, Stony Brook, NY, USA
[2]Dept of Biomedical Engineering, Wright State University, Dayton, OH, USA
[3]Quantum Opus LLC
[4]Dept of Neurosurgery, Stony Brook University, Stony Brook, NY, USA
[5]Dept of Neurology & Rehabilitation Medicine, University of Cincinnati, Cincinnati, OH, USA
**ulas.sunar@stonybrook.edu*

Abstract: This study evaluates the feasibility of depth-sensitive bedside monitoring of cerebral blood flow (CBF) and low-frequency oscillations (LFOs) using time-domain diffuse correlation spectroscopy (TD-DCS) in healthy controls and patients with disorders of consciousness (DOC). A 1064 nm TD-DCS system equipped with superconducting nanowire single-photon detectors (SNSPDs) was used to collect 10-minute resting-state data from 25 healthy adults and 5 patients with traumatic brain injury (TBI) diagnosed with DOC, including minimally conscious state (MCS) and coma, in the subacute phase. Photon arrival times were temporally gated to distinguish superficial and cortical-weighted tissue contributions. The blood-flow index (BFI) was extracted from gated autocorrelation functions, and LFOs were quantified using power spectral density within the Slow-5 (0.01-0.027 Hz), Slow-4 (0.027-0.073 Hz), and Slow-3 (0.073-0.198 Hz) bands. Compared to healthy controls, DOC patients exhibited altered resting-state LFO amplitude and spectral distribution, suggestive of altered neurovascular dynamics in severe brain injury. An auditory “smile” command was delivered to five healthy subjects, one MCS patient, and one unresponsive wakefulness syndrome (UWS) patient to assess task-evoked hemodynamic responses. During the task, healthy participants showed clear hemodynamic responses, whereas DOC patients demonstrated attenuated and more transient responses. Overall, TD-DCS provides a noninvasive, depth-resolved approach for assessing cerebral hemodynamics and residual cortical responsiveness, supporting its potential for bedside neurocritical-care monitoring.

Keywords: cerebral blood flow; disorders of consciousness; low-frequency oscillations; time-domain diffuse correlation spectroscopy; traumatic brain injury.

Introduction

Acute brain injury (ABI) is a leading cause of mortality and long-term disability, particularly among young adults [1–4] . While the primary injury occurs at the moment of trauma, secondary processes such as impaired autoregulation, ischemia, and inflammation can evolve over hours to days, driving further neurological deterioration [5,6]. Continuous bedside monitoring of cerebral blood flow (CBF) is therefore highly desirable for detecting secondary injury and guiding timely intervention [7–13]. Conventional imaging techniques such as magnetic resonance imaging (MRI), computed tomography (CT), and positron emission tomography (PET) provide detailed structural and functional information but are limited by their high cost, logistical complexity, and lack of feasibility for continuous bedside monitoring [14]. Diffuse correlation spectroscopy (DCS) offers a non-invasive and portable alternative capable of tracking microvascular CBF in real time. Compared to near-infrared spectroscopy (NIRS), DCS provides greater sensitivity to cerebral blood flow and has shown promise in neurocritical care applications [11,15,16]. However, standard continuous-wave (CW) DCS systems are limited in depth specificity and can be influenced by signals from superficial tissues such as the scalp and skull [17–19].

Time-domain DCS (TD-DCS), enhances depth sensitivity by isolating late-arriving photons that have traveled deeper into tissue [20–22]. When implemented at longer wavelengths such as 1064 nm and combined with highly sensitive detectors such as SNSPDs, TD-DCS enables deeper penetration, improved signal-to-noise ratio, and higher permissible laser power, making it well-suited for adult human brain monitoring [23–33]. While cerebral blood flow parameter provides one indication of brain health, spontaneous low-frequency oscillations (LFOs) in the range of 0.01-0.2 Hz are known to reflect important physiological processes including endothelial, neurogenic, and respiratory activity, and have been associated with cerebrovascular regulation and brain function [31,34–53]. Optical bedside monitoring of cerebral hemodynamics in brain injury has been demonstrated using DCS (e.g.,[54–56,56–65]). However, few studies have focused on low-frequency oscillations (LFOs), and their depth-specific characterization in acute human brain injury remains largely unexplored.

Disorders of Consciousness (DOCs) represent a clinical spectrum of severe cerebral dysfunction, encompassing coma and chronic states of impaired consciousness. These chronic states include the Unresponsive Wakefulness Syndrome (UWS) (formerly known as the Vegetative State), characterized by preserved arousal with no evidence of purposeful behavior or awareness, and the Minimally Conscious State (MCS), defined by inconsistent but reproducible signs of awareness, such as visual tracking, localization, or command following [66, 67] .

While resting-state signals and oscillations can provide insight into baseline physiology, task-evoked functional responses may offer greater contrast for assessing consciousness states by detecting residual cortical reactivity. Auditory or command-driven paradigms such as familiar voices or simple motor tasks elicit reproducible hemodynamic responses in conscious patients but are absent in deeply unconscious states[45,68–70] . These paradigms are commonly studied with functional MRI (fMRI), which is impractical in intensive care unit (ICU) settings. In this study, we incorporated auditory stimulation tasks, which elicit reproducible hemodynamic responses in patients with residual consciousness [45–53,68]. In the present study, task-based auditory stimulation is included primarily as a qualitative illustration of depth-sensitive TD-DCS signal behavior, rather than as a primary marker of cognitive function or motor planning.

Time-domain diffuse correlation spectroscopy (TD-DCS) addresses these limitations by directly measuring cerebral blood flow (CBF) and its spontaneous fluctuations in a depth-sensitive, non-invasive manner. Unlike NIRS- or BOLD-based techniques that rely on surrogate markers of oxygenation, TD-DCS quantifies microvascular flow dynamics with high temporal resolution and deep-tissue sensitivity when implemented at 1064 nm with superconducting nanowire single-photon detectors. This configuration enables deeper tissue penetration, improved signal-to-noise ratio, and higher laser safety limits, making it a realistic alternative to fMRI in longitudinal consciousness assessment and neurocritical-care monitoring [10,71–78] .

By combining the portability and bedside practicality of fNIRS and EEG with the physiological specificity of perfusion imaging, TD-DCS offers a unique opportunity for repeated, real-time assessment of brain function in DOC patients without requiring transport or complex infrastructure. In this study we evaluate the utility of TD-DCS in both resting-state and task-evoked paradigms to detect residual cortical reactivity and differentiate levels of consciousness in critically ill patients as a potential bedside adjunct for neurocritical-care monitoring.

Materials and Methods

Study Design and Patient Details

This study is a retrospective analysis of a prospective observational protocol designed to evaluate cerebral blood flow (CBF) in healthy individuals and patients with traumatic brain injury (TBI). A total of 25 healthy adults (14 males, 11 females; mean age 26.9 ± 4.8 years) were recruited for resting-state measurements, and an additional cohort of five healthy subjects (5 males; mean age 29.0 ± 5.5 years) participated in an auditory "smile" task to assess task-evoked hemodynamic responses. The auditory "smile" task consisted of repeated verbal commands ("smile") delivered at fixed intervals to elicit cortical hemodynamic activation, as described below.

Six TBI patients were enrolled between 2022 and 2025 from the University of Cincinnati Medical Center and Stony Brook University Hospital. Of these, five patients (two diagnosed with minimally conscious state [MCS] and three with coma) underwent resting-state TD-DCS measurements. One additional patient diagnosed with unresponsive wakefulness syndrome (UWS) underwent task-based TD-DCS measurements only, using a bilateral probe configuration. A summary of subject diagnoses, clinical characteristics, and experimental inclusion is provided in Supplementary Table S1. For resting-state analyses, patients diagnosed with MCS (n = 2) and coma (n = 3) were analyzed together as a DOC cohort due to the limited sample size of individual diagnostic subgroups. Task-based measurements in DOC patients are presented descriptively at the individual-subject level.

Resting-state recordings consisted of a single 10-minute acquisition performed in the intensive care unit (ICU) during routine clinical care. Task-based recordings consisted of an auditory "smile" command delivered approximately every 60 seconds for a total of five repetitions [79–81]. No experimental interventions were introduced, and no restrictions were placed on medical treatment during the data acquisition period. All healthy participants provided written informed consent under protocols approved by the Institutional Review Boards (IRBs) of Wright State University and Stony Brook University. The study was conducted in accordance with the Declaration of Helsinki and approved by the IRBs of Wright State University, Stony Brook University, and the University of Cincinnati Medical Center. For TBI patients, informed consent was obtained from legally authorized representatives in accordance with these IRB approvals.

TD-DCS System for Data Acquisition

Figure 1. Overview of the time-domain diffuse correlation spectroscopy (TD-DCS) system. a) Quantum Opus superconducting nanowire single-photon detector (SNSPD) system with the VisIR pulsed laser (1064 nm) mounted on top. The display shows the photon distribution of time-of-flight (DTOF). b) Close-up view of the custom 3D-printed probe with a 15 mm source-detector separation between the source and detector fibers. c) Example of the probe placed on the right forehead of a human subject for cerebral blood flow measurements.

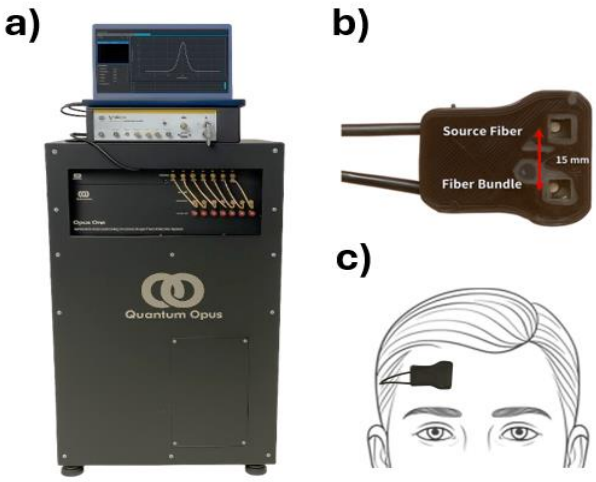

The TD-DCS method has been employed in numerous previous studies, demonstrating its feasibility for clinical use [82–91] . Figure 1a-c illustrates the components of the system and probe placement**.** The optical imaging probe was positioned on the right forehead, between EEG scalp locations F4 and F8, to ensure consistent and anatomically relevant placement. The probe incorporated a 600-μm-core multimode source fiber (NA = 0.39, FT600EMT, Thorlabs, NJ, USA) and an 8.2-μm-core detector fiber (SMF-28, Thorlabs, NJ, USA), which is few-mode at 1064 nm[92]. The source-detector separation (SD) was fixed at 15 mm, a deliberate choice reflecting the established TD-DCS trade-off between cortical-weighted sensitivity and photon statistics, in which depth sensitivity is governed primarily by photon time-of-flight and further enhanced through late temporal gating rather than separation alone [17,18,21,23]. All fibers were aligned through a 5 mm right-angled prism and embedded in a custom-designed, flexible 3D-printed housing optimized for ergonomic use in clinical environments. The probe's contact footprint was approximately 25 mm × 25 mm, slightly larger than a US quarter, minimizing scalp contact while enabling secure and reproducible placement. The assembly was affixed using medical-grade Tegaderm film (3M, Saint Paul, MN) following sterilization with alcohol swabs. Reflected photons at 1064 nm were detected using four superconducting nanowire single-photon detectors (SNSPDs), which were interfaced with a 4-channel time-correlated single-photon counting (TCSPC) system (HydraHarp400, PicoQuant GmbH, Berlin, Germany) [93,94]. During the initial phase of the study, the healthy resting-state cohort (H1-H25) and one comatose TBI patient (Coma-1) measured at the University of Cincinnati Medical Center, a 1064 nm pulsed seed laser (QC2D106P-64D0, QDLaser Inc.,

Kanagawa, Japan) operating at an 80 MHz repetition rate with a 250 ps pulse width was used. For all remaining subjects, including patients with disorders of consciousness, as well as for all functional task ("smile") measurements, a 1064 nm pulsed laser (VisIR-1064-HC High-Coherence, PicoQuant GmbH, Berlin, Germany) operating at an 80 MHz repetition rate with a 400 ps pulse width was used. The beam exiting the prism face was expanded to approximately 4.5 mm in diameter using a diffuser film to ensure uniform illumination across a large beam area. The average power was kept below ANSI safety limits, and each detection channel operated at a photon count rate of ~1×10^7 counts per second (cps).

Data Analysis

The analyses below were designed to test protocol-specific hypotheses regarding depth-resolved resting-state dynamics and task-evoked depth-dependent hemodynamic signals.

Resting-State Analysis

Time-tagged photon arrival data were recorded continuously. Resting-state measurements consisted of a single 10-minute acquisition per subject. Data processing was performed using a custom MATLAB routine on a high-memory computing node with 1.5 TB of RAM. The instrument response function (IRF) was characterized by placing a thin scattering layer (Teflon tape, 3M) between the source and detector fibers during a 30-second calibration, resulting in a full width at half maximum (FWHM) of ~400 ps for the VisIR-1064-HC [95] . Two temporal gates were selected based on the distribution of time-of-flight (DTOF). The early gate (EG), centered at 0.20 ns with a width of 100 ps, was positioned just after the DTOF peak to emphasize photons that predominantly sampled superficial tissue layers (Fig. 2a). The late gate (LG), centered at 1.03 ns with a width of 250 ps, was placed on the decaying slope of the DTOF to enhance sensitivity to deeper tissue regions (Fig. 2d). Figure 2 illustrates these gating definitions using data from a representative comatose patient**.** Gate positions were defined relative to the peak of the combined DTOF across all channels to maintain consistent depth sensitivity among subjects. This strategy was designed to capture photons from deeper tissue layers while minimizing contamination from superficial dynamics. It aligns with prior findings that optimally selected narrow time gating (e.g., 100 ps) with sufficient SNR can enhance depth specificity in TD-DCS [96]. As motivated by Tagliabue *et al* [97], who demonstrated spatial and temporal optical heterogeneity in injured brains, we performed subject-specific fitting of the temporal point spread function (TPSF) to extract the absorption (μ_a) and reduced scattering (μ_s') coefficients, which were then used as fixed *a priori* inputs for the analytical intensity autocorrelation function (g_2) fitting to quantify the blood flow index

(BFI). The TPSF fitting was performed using an analytical solution of the time-domain diffusion equation in reflectance geometry assuming a semi-infinite homogeneous medium with extrapolated boundary conditions [98,99].

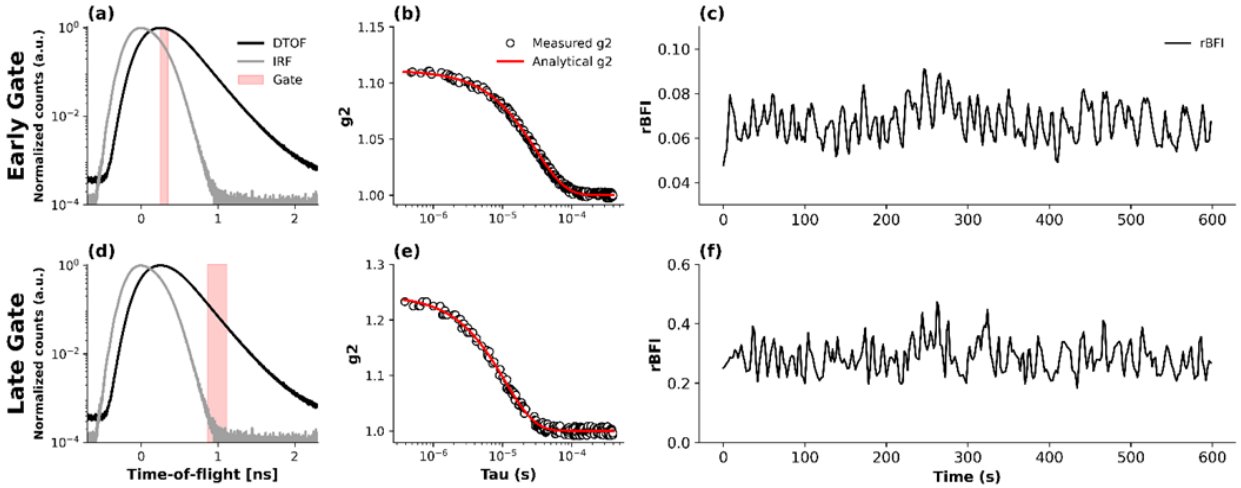

Figure 2. Early- and late-gate TD-DCS analysis for a representative comatose patient. (a,d) Normalized distributions of time-of-flight (DTOF, black) and instrument response function (IRF, gray), with the selected gate window shown in red for the early and late gates, respectively. (b,e) Corresponding normalized intensity autocorrelation curves $g_2(\tau)$ (black circles) and analytical fits (red lines) used to estimate the blood-flow index (BFI). (c,f) Temporal evolution of the relative blood-flow index (rBFI) derived from the early and late gates, respectively, showing increased fluctuation amplitude and deeper sensitivity for the late-gate signal.

Under this modeling framework, the extracted optical properties should be interpreted as effective bulk parameters that reflect the weighted contribution of all tissues sampled by the photon time-of-flight distribution, rather than depth-resolved or layer-specific tissue properties. This approach accounts for inter-subject variability in optical properties, which is particularly relevant in TBI patients where extracerebral tissue characteristics may vary substantially. Representative TPSF and IRF fits for healthy, MCS, and comatose subjects are provided in Supplementary Fig. S1 to illustrate fitting quality; optical property values are shown for completeness and are not interpreted or compared across diagnostic groups. The g_2 functions were extracted directly from each temporal gate using delay times ranging from 5×10^{-7}s to 1×10^{-3} s. Autocorrelations were calculated using 5 s integration windows with 1 s step size, producing overlapping data segments to enhance temporal resolution (Figs. 2b, e). The resulting g_2 curves were fitted to an analytical

model derived from the time-domain diffusion equation assuming a semi-infinite homogeneous medium geometry [17,20,100]. Although this geometry does not explicitly model layered head anatomy or depth-resolved photon trajectories, depth sensitivity was achieved experimentally through time-of-flight–based temporal gating, with the late gate providing increased sensitivity to deeper cerebral tissue and reduced sensitivity to extracerebral contributions. Because detection was performed with an 8.2 μm-core few-mode fiber, the measured coherence factor (β) values were lower than those typically obtained in single-mode DCS systems (β ≈ 0.5), resulting in smaller g_2 amplitudes (Figs. 2b, e). Although this configuration reduces temporal coherence, it substantially improves the signal-to-noise ratio (SNR), which is critical for reliable estimation of cerebral blood flow in human measurements. Final relative blood-flow index (rBFI) values were obtained by fitting g_2 curves averaged across all four detection channels (Figs. 2c, f). For resting-state measurements, absolute BFI time series were used to compute mean flow values and low-frequency oscillation (LFO) metrics.

Spectral Analysis of Low-Frequency Oscillations (LFOs)

In addition to evaluating cerebral blood flow changes, we analyzed LFOs in the blood flow index as potential indicators of cerebrovascular function. LFOs were defined as spontaneous fluctuations occurring below 0.5 Hz and were examined within three descriptive frequency bands (Slow-5, Slow-4, and Slow-3), as summarized in Table 1. This frequency-band nomenclature follows prior resting-state fMRI and optical neuroimaging literature [34,48,101–106], where low-frequency oscillations are commonly subdivided into Slow-5, Slow-4, and Slow-3 bands for spectral characterization[101–103]. Consistent with common fMRI and fNIRS practice, the broader low-frequency range (≈0.01-0.1 Hz) is generally interpreted as reflecting neurovascular coupling in aggregate; the subdivision into Slow-5, Slow-4, and Slow-3 bands is used here to facilitate comparative, depth-resolved spectral analysis rather than to imply distinct or exclusive physiological generators. Bands I and II are listed in Table 1 for completeness but were not analyzed or interpreted separately in this study; band-specific comparisons focus on Slow-5, Slow-4, and Slow-3 (Bands V-III).

Prior to spectral analysis, the resting-state BFI time series were detrended using a second-order polynomial to remove slow baseline drifts. The signals were then band-pass filtered between 0.01 and 0.4 Hz using a zero-phase Butterworth filter (2nd order) to isolate low-frequency oscillations while avoiding phase distortion. Power spectral density (PSD) was computed using the fast Fourier transform (FFT) applied to the full 10-minute resting-state BFI time series for each subject. The total amplitude of low-frequency oscillations was quantified using the

amplitude of low-frequency fluctuations (ALFF), defined as the square root of the integrated PSD over the 0.01-0.4 Hz range**.** To compare spectral shapes across subjects, each PSD was normalized by its own total low-frequency power and interpolated onto a common frequency axis between 0.01 and 0.4 Hz (see Figs. 3c, g for representative group-averaged normalized PSDs). A sensitivity analysis examining the effect of the PSD normalization bandwidth on normalized spectral estimates is provided in Supplementary Fig. S2. Because PSD.n and LFO.n are normalized by the total 0.01-0.4 Hz power, these metrics describe spectral redistribution (band reorganization) rather than absolute oscillation amplitude.

Band-limited power in each LFO range (P_B) was obtained by integrating the unnormalized PSD over the corresponding frequency interval. Normalized band power was defined as $R_B = P_B/P_{\text{total}}$, where P_{total} is the total integrated PSD over 0.01-0.4 Hz; thus R_B represents the fraction of total 0.01-0.4 Hz BFI power allocated to Slow-5, Slow-4, or Slow-3.

Mean and standard error of P_{total} and R_B were calculated for both the healthy control group and the DOC cohort (n = 5). The summary statistics are reported for descriptive purposes only, and individual subject values are explicitly visualized to reflect inter-subject variability in the context of the limited sample size.

We note that arterial blood pressure (ABP) was not recorded in this feasibility study. Unlike transfer-function analyses of autoregulation that require ABP as an input signal (e.g., [107–112]), our approach focuses on the output fluctuations of the TD-DCS blood-flow index and on the relative distribution of power across physiologically motivated frequency bands.

Table-1: Frequency bands for low-frequency oscillations (LFOs) with respect to band-1 to band-5, and their associated descriptor.

Band	**Frequency Range (Hz)**	**Descriptor**
V	0.01-0.027	Very-low-frequency LFO
IV	0.027-0.073	Low-frequency LFO
III	0.073-0.198	Higher low-frequency LFO
II	0.198-0.5	Higher-frequency physiological range / respiration contaminated
I	0.5-0.75	Higher-frequency physiological range / noise

Task-Based (Auditory "Smile") Measurements

Task-based recordings consisted of an auditory "smile" command delivered approximately every 60 s for a total of five repetitions, resulting in an acquisition duration of approximately 5 min per subject. For task-based analyses, relative blood-flow index (rBFI), defined as BFI normalized to a pre-stimulus baseline, was used to characterize stimulus-evoked hemodynamic responses. Task-based analyses were performed to explore whether stimulus-evoked cortical hemodynamic responses observed in healthy subjects could also be detected at the individual-subject level in patients with disorders of consciousness, including MCS and UWS.

Early-gate and late-gate rBFI time series were detrended and band-pass filtered to suppress slow baseline drift and high-frequency noise while preserving task-relevant dynamics. Expected stimulus onset times were defined based on the experimental protocol, and peri-stimulus windows were extracted for each trial. Local maxima in EG and LG signals were identified within predefined temporal search windows following stimulus onset to account for inter-subject variability in response timing. Extracted trials were baseline-corrected using a pre-peak interval and averaged within each subject.

Because late-gate TD-DCS measurements are inherently low signal-to-noise due to reduced photon counts at longer time-of-flight, particularly in clinical bedside measurements, a state-space modeling approach was employed to robustly infer the latent cortical hemodynamic response. The observed LG rBFI signal was modeled as a combination of a latent task-evoked response and a superficial contribution proportional to the EG signal. The latent response was represented using a set of Gaussian basis functions convolved with the stimulus time course. A Kalman filter with Rauch-Tung-Striebel smoothing was applied to estimate the underlying latent state by combining temporal continuity constraints with measurement uncertainty [113,114]. In this formulation, the latent state comprised task-evoked hemodynamic response weights and a time-varying superficial coupling coefficient, while the observation model related these latent variables to the measured late-gate rBFI signal. The inferred LG signal, with superficial contributions regressed out to reduce extracerebral contamination, was used for subsequent block averaging and descriptive comparison across subjects.

Results

Resting-State and Task-Based TD-DCS Measurements

Resting-State Cerebral Blood Flow and LFOs: Healthy vs DOC

Resting-state TD-DCS measurements were obtained from healthy controls (n = 25) and from patients with disorders of consciousness (DOC; n = 5), including individuals diagnosed with minimally conscious state and coma. Only subjects who completed resting-state recordings were included in this analysis; task-only subjects were excluded. In particular, the post-surgical unresponsive wakefulness syndrome (UWS) patient who participated only in the auditory task was not included in the resting-state analysis.

Depth sensitivity was achieved using time-of-flight-based temporal gating, with the early gate (EG) preferentially sampling superficial tissues and the late gate (LG) providing enhanced sensitivity to deeper, cortical-weighted signals **(Fig. 3a, e).** Mean blood-flow index (BFI), used here as a proxy for cerebral blood flow, was summarized descriptively for both groups, with individual subject values explicitly shown for the DOC cohort. In the superficial compartment (EG; **Fig. 3a),** DOC patients exhibited descriptively higher BFI values compared to healthy controls, accompanied by substantial inter-subject variability. A similar pattern was observed in the cortical-weighted compartment **(LG; Fig. 3e),** where DOC patients again demonstrated elevated BFI relative to healthy participants. These observations suggest altered baseline perfusion dynamics in disorders of consciousness, though no statistical inference is made due to the limited patient sample size. Low-frequency oscillations (LFOs) in the resting-state BFI signal were further examined using the amplitude of low-frequency fluctuations (ALFF; 0.01-0.4 Hz) to assess depth-dependent oscillatory dynamics. In the superficial compartment **(EG; Fig. 3b),** healthy participants exhibited descriptively higher ALFF values compared to the DOC cohort, whereas in the cortical-weighted compartment **(LG; Fig. 3f),** group differences were less pronounced, with overlapping values observed across subjects.

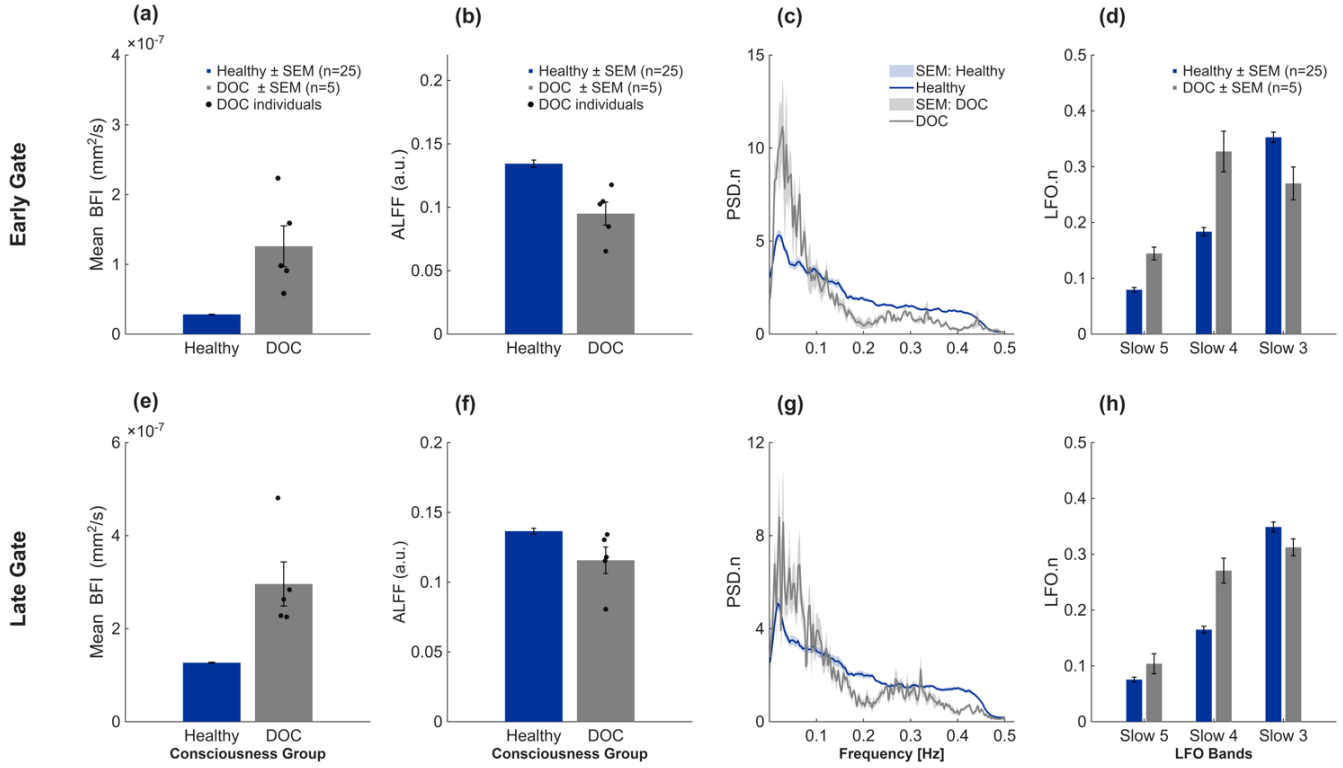

Figure 3. Depth-resolved resting-state cerebral blood flow and low-frequency oscillations in healthy controls and patients with disorders of consciousness. (a-d) Early-gate (EG) results, preferentially weighted toward superficial tissues. (e-h) Late-gate (LG) results, providing enhanced sensitivity to deeper (cortical-weighted) signals. (a,e) Mean absolute blood-flow index (BFI, mm²/s). (b,f) Amplitude of low-frequency fluctuations (ALFF; 0.01-0.4 Hz). (c,g) Normalized power spectral density (PSD.n) of the resting-state BFI signal (mean ± SEM). (d,h) Normalized band-limited LFO power (LFO.n), defined as the fraction of total 0.01-0.4 Hz power contained within Slow-5 (0.01-0.027 Hz), Slow-4 (0.027-0.073 Hz), and Slow-3 (0.073-0.198 Hz). Bars indicate group mean ± SEM for healthy controls (n = 25) and DOC patients (n = 5; minimally conscious state and coma); black markers denote individual DOC subjects in panels (a,b,e,f). Results are presented descriptively due to the limited DOC sample size.

Normalized power spectral density analyses (PSD.n; **Fig. 3c, g)** revealed systematic depth-dependent spectral reorganization. Healthy controls exhibited a broader distribution of power across the low-frequency range, while DOC patients showed a relative shift toward very low

frequencies (< 0.1 Hz), particularly in cortical-weighted late-gate measurements. This pattern indicates a greater concentration of spectral power at frequencies below 0.1 Hz in the DOC cohort, particularly in late-gated measurements. Normalized band-limited LFO metrics (LFO.n; Fig. 3d,h) further quantified this spectral distribution. Healthy participants demonstrated relatively greater contributions from higher-frequency LFO components, whereas DOC patients exhibited increased dominance of slower oscillatory bands. Together, these findings show descriptively different baseline blood-flow magnitude and low-frequency oscillatory structure between healthy controls and the DOC cohort, with depth-dependent differences observed across early- and late-gated signals.

Illustrative Depth-Sensitive Hemodynamic Signals During Auditory Stimulation

To qualitatively assess depth-dependent hemodynamic sensitivity during a task paradigm, we analyzed early- and late-gated TD-DCS responses during an auditory stimulation protocol in healthy controls (n = 5) and a patient diagnosed with unresponsive wakefulness syndrome (UWS; n = 1). Early- and late-gated measurements were interpreted as being differentially weighted toward superficial extracerebral and deeper cerebral tissue compartments, respectively, consistent with prior time-domain optical studies exploiting photon time-of-flight information and depth-sensitive observables to reduce superficial contamination [115,116]. Task-locked responses were estimated using a Kalman-based regression framework with the stimulation paradigm as a regressor, followed by trial-wise baseline correction and block averaging.

Early-Gated Signals

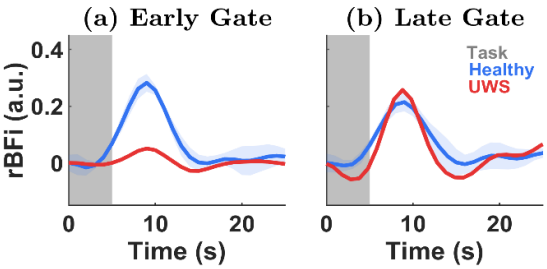

Figure 4. Depth-sensitive TD-DCS responses during a 5-s auditory stimulation task. Early gated (a) and late gated (b) relative blood flow index (rBFI) responses in healthy controls (blue, mean ± SEM) and a UWS patient (red). Shaded region indicates the 5-s task period.

411 In healthy subjects, early gated signals exhibited large, task-locked increases in relative blood
412 flow index (rBFI), with peak amplitudes occurring during the stimulation window (Fig. 4.a). These
413 responses were robust across trials and substantially larger than corresponding late-gated
414 signals. Given the strong sensitivity of early-arriving photons to superficial tissue layers, these
415 pronounced task-locked EG responses are consistent with extracerebral physiological
416 contributions, including scalp and autonomic vascular responses, as widely reported in time-
417 domain fNIRS and diffuse optical studies[115–117]. In contrast, the UWS patient demonstrated
418 minimal modulation in early-gated rBFI during auditory stimulation, with signals remaining near
419 baseline throughout the task period. This absence of early-gated task reactivity is consistent with
420 reduced superficial physiological engagement during stimulation and further highlights the
421 sensitivity of EG TD-DCS measurements to superficial rather than cerebral hemodynamic
422 changes.
423
424 **Late-Gated Signals**
425 Late-gated (LG) signals exhibited smaller-amplitude but structured task-locked dynamics in both
426 healthy subjects and the UWS patient (Fig. 4. b). Compared to early-gated measurements, late-
427 gated responses were temporally smoother and showed reduced variability, consistent with
428 increased weighting toward deeper tissue compartments and reduced sensitivity to superficial
429 physiology. This behavior closely parallels prior time-domain optical findings demonstrating that
430 depth-weighted or late-photon observables substantially suppress task-locked superficial
431 contributions present in attenuation-based or early-weighted measurements [115,118].
432 Notably, the UWS patient exhibited late-gated response amplitudes comparable to, and in some
433 instances exceeding, those observed in healthy controls. Similar increases in hemodynamic
434 response amplitude in UWS relative to healthy subjects have been reported in prior neuroimaging
435 studies and interpreted as reflecting altered or dysregulated neurovascular coupling rather than
436 preserved cognitive processing[119]. Accordingly, these late-gated task responses are presented
437 descriptively and interpreted cautiously.
438
439 **Discussion**
440 Accurate differentiation between UWS and MCS remains difficult, with misdiagnosis rates of 30–
441 40% when relying solely on clinical examination [45,120–122]. Neuroimaging and neurophysiological
442 modalities, including fMRI [79,123,124], PET [125–128], EEG [126,126,129,129,130,130–133], and NIRS [80,134–136],
443 have enabled detection of MCS/covert consciousness, in which patients demonstrate preserved
444 cortical activation despite absent behavioral output. However, these techniques are limited by

either lack of portability (fMRI, PET) or depth specificity (EEG, NIRS), constraining their feasibility for repeated bedside assessments in critically ill patients. Electroencephalography (EEG) provides bedside compatibility and high temporal resolution but suffers from low spatial specificity, susceptibility to artifacts, and reduced sensitivity to deep cortical responses, particularly in patients with skull defects [132,137,138]. Functional NIRS has recently shown promise in detecting task-evoked responses using personalized motor-speech imagery and covariance-based classifiers [139–141], yet it remains limited by superficial contamination and reliance on surrogate oxygenation measures. In this context, there remains a need for a portable, depth-sensitive method capable of assessing cerebral physiology at the bedside.

This study demonstrates a novel application of TD-DCS for depth-sensitive assessment of CBF and spontaneous LFOs in healthy individuals and patients with TBI diagnosed with disorders of consciousness (DOC). Using a portable 1064 nm TD-DCS system with SNSPDs, we obtained depth-specific hemodynamic signatures that distinguish superficial and cortical-weighted vascular dynamics [26,27,142]. Given the limited sample size of individual diagnostic subgroups, resting-state findings are interpreted at the level of healthy controls versus a combined DOC cohort, and observations within DOC patients are treated as descriptive rather than inferential.

Compared to healthy controls, DOC patients exhibited altered resting-state LFO characteristics in both early- and late-gated signals, with larger shifts in the early gate and attenuated but directionally consistent redistribution trends in the late gate. In our cohort, ALFF tended to be lower in DOC patients in both gates, while normalized spectral analyses demonstrated increased relative weighting of very low frequencies (<0.1 Hz) and greater Slow-5/Slow-4 fractions with reduced Slow-3 contribution. These observations are broadly consistent with prior fNIRS and fMRI studies reporting disrupted resting-state hemodynamic oscillations and altered neurovascular dynamics in severe brain injury and disorders of consciousness (e.g. [80,143–145]). In particular, optical and fMRI studies such as Schulthess et al.[81] and Kazazian et al.[80] have reported reduced spontaneous or task-evoked low-frequency activity in unresponsive wakefulness syndrome, supporting the interpretation that preserved LFO may reflect residual neurovascular reactivity and cortical viability. These findings contrast with acute-phase animal studies (e.g., White et al.[146]), which reported increased LFOs shortly after injury, potentially reflecting metabolic instability and/or pathological vasomotion during the hyperacute phase. In the subacute clinical setting of the present study, the observed spectral slowing and redistribution of LFO content may be more consistent with dysregulated vasomotor control and altered vasomotor control and altered neurovascular regulation rather than acute hyperacute increases or inflammation. While DOC

patients demonstrated heterogeneous resting-state profiles, no statistical separation between minimally conscious and comatose patients is inferred from the present data due to the limited subgroup sizes. Instead, the observed inter-subject variability highlights the complexity of cerebrovascular dysfunction following severe brain injury and underscores the need for larger cohorts to determine whether depth-resolved spectral metrics can reliably differentiate diagnostic categories or track recovery trajectories.

Mean BFI was higher in late-gated signals than in early-gated measurements, particularly in DOC patients. Low-frequency spectral features were observed in both gates, with larger shifts in the early gate and attenuated but directionally consistent redistribution trends in the late gate. The observed elevation in baseline BFI in DOC patients is interpreted cautiously and is not attributed to preserved neural activity. Instead, increased BFI may reflect altered cerebrovascular tone and dysregulated neurovascular control after severe brain injury, including impaired autoregulatory mechanisms and disrupted flow-metabolism coupling, as well as systemic influences (e.g., ventilation/$PaCO_2$, sedation, vasoactive medications). Similar elevations in baseline CBF or perfusion have been reported in subacute TBI and disorders of consciousness and are often interpreted as reflecting dysregulated cerebrovascular control rather than task-evoked functional activation [11,32,147].

In contrast, normalized low-frequency spectral metrics (PSD.n and LFO.n) emphasize how the remaining fluctuations are distributed across frequencies and therefore support interpretation in terms of spectral reorganization. Such alterations in low-frequency spectral content have been associated with altered autoregulation and vasomotor dysregulation in prior optical studies [38,41,43,45,50,51,53,148]. Both early and late gates showed depth-dependent spectral redistribution across LFO bands, with larger shifts in the early gate and similar but attenuated trends in the late gate. The persistence of these trends in the late gate is consistent with a deeper-weighted contribution and highlights the utility of time-gating for separating superficial-weighted and cortical-weighted dynamics in neurocritical-care applications. In addition to resting-state analysis, we evaluated functional reactivity using a brief auditory “smile” protocol. The task-based TD-DCS results further illustrate the differential sensitivity of early- and late-gated measurements to superficial versus depth-weighted hemodynamic contributions. In healthy subjects, large task-locked responses observed in the early gate are consistent with the strong sensitivity of early-arriving photons to superficial extracerebral physiology, which may include autonomic or arousal and systemic coupling effects during task engagement. The absence of comparable early-gated modulation in the UWS patient suggests the dependence of early-gated signals on superficial

physiological engagement rather than cerebral hemodynamics. In contrast, late-gated signals exhibited lower amplitude and smoother temporal dynamics across both groups, consistent with increased weighting toward deeper tissue compartments and partial suppression of superficial contributions. The presence of structured late-gated responses in the UWS patient, with amplitudes comparable to or exceeding those observed in healthy controls, is consistent with prior neuroimaging studies reporting altered hemodynamic responses in disorders of consciousness [80,149]. Such responses have been interpreted as reflecting dysregulated neurovascular coupling or altered cerebrovascular dynamics rather than preserved cognitive or motor processing. Importantly, these task-based findings are presented descriptively and are not intended to infer localized cortical activation, motor planning, or functional network engagement. Instead, they serve to qualitatively demonstrate how photon time-of-flight gating alters task-locked signal behavior in TD-DCS measurements in brain-injured patients. Together with the resting-state LFO analyses, these results emphasize the importance of depth-sensitive approaches for interpreting optical hemodynamic signals in both healthy and severely brain-injured populations.

Together, these results highlight the potential of TD-DCS to provide real-time, depth-resolved assessment of cerebral hemodynamic dynamics and neurovascular integrity in critically ill patients at the bedside. The ability to non-invasively measure cerebral LFOs and task- or state-related BFI fluctuations at the bedside has significant clinical implications. Current neuro-monitoring tools in the ICU are either invasive (e.g., intracranial pressure monitors), lack depth sensitivity (e.g., NIRS), or are not practical for continuous use (e.g., MRI, PET). TD-DCS bridges this gap by offering portable, real-time monitoring of both baseline perfusion and depth-weighted hemodynamic signals. In neurocritical care, LFO patterns may serve as indicators of cerebrovascular health, injury severity, and recovery potential [42,45,51]. Longitudinal tracking of LFOs and hemodynamic responses could help clinicians identify patients at risk of secondary injury, evaluate the effectiveness of therapeutic interventions, and guide decisions around sedation, rehabilitation, and prognosis.

While our findings are promising, several limitations warrant consideration. The patient data are limited to five TBI cases, which restricts generalizability. Given the small MCS sample size (n = 2), group-level resting-state findings should be interpreted as preliminary and descriptive; larger cohorts will be required to assess the impact of focal pathologies such as hemorrhage on depth-resolved hemodynamic metrics**.** Larger cohorts are needed to validate LFO spectral changes as reliable markers of injury severity and recovery. Although time-gating improves cerebral sensitivity, residual contamination from superficial tissues cannot be fully ruled out. Similarly,

544 optical properties (μ_a, μ_s') estimated from time-resolved TPSF fitting using a homogeneous semi-
545 infinite diffusion model should be interpreted as effective bulk parameters reflecting the weighted
546 contribution of both superficial and cerebral tissues. In patients with prior cranial surgery, such as
547 the MCS case included here, extracerebral structural alterations may influence the fitted μ_s' values
548 and should not be interpreted as direct markers of cortical microstructure [150,151]. The β values
549 derived from our g_2 fits were lower than standard CW-DCS systems due to the use of few-mode
550 fibers, although it enabled sufficient photon throughput for feasibility of human brain
551 measurements. Prior optical studies used ABP as an input function to assess autoregulation
552 through transfer-function analysis [108,110,148,152–156] . In this feasibility study, ABP was not recorded,
553 so our interpretation relied on the output signal of TD-DCS. By normalizing PSD to total power,
554 we focused on the relative distribution of oscillatory activity across bands. While this approach
555 does not capture input-output coupling, it provides complementary information on depth-
556 dependent cerebrovascular dynamics. Future work will incorporate systemic inputs for a more
557 complete assessment of autoregulation. Combining TD-DCS with other modalities such as EEG
558 or fNIRS may enhance spatial resolution and signal interpretation [38,111,112,157–159] . Future hardware
559 development could explore optimized geometries that maintain high count rates while covering
560 more spatial coverage. Longitudinal studies will be important to test whether TD-DCS metrics
561 track recovery or deterioration over time.
562

563 **Conclusions**

564 This study demonstrates the utility of time-domain diffuse correlation spectroscopy (TD-DCS) as
565 a non-invasive, depth-sensitive approach for monitoring cerebral blood flow (CBF) and
566 spontaneous low-frequency oscillations (LFOs) in the human brain. Resting-state analyses
567 revealed altered depth-resolved LFO characteristics in patients with acute brain injury and
568 disorders of consciousness compared with healthy controls, with larger shifts in early-gated
569 signals and attenuated but directionally consistent redistribution trends in late-gated signals.
570 These findings are suggestive of altered cerebrovascular regulation following severe brain injury.
571 By exploiting photon time-of-flight information, TD-DCS enabled separation of superficial and
572 deeper hemodynamic contributions, highlighting the importance of depth-sensitive measurements
573 for accurate interpretation of optical signals in neurocritical care. Task-based measurements were
574 included as a qualitative illustration of depth sensitivity and demonstrated distinct early- and late-
575 gated signal behavior, without implying localized cortical activation or preserved cognitive
576 function. Together, these results underscore the potential of TD-DCS as a portable bedside tool

for depth-resolved assessment of cerebral hemodynamics and vascular dynamics in critically ill patients. With further technical refinement and validation in larger cohorts, TD-DCS may complement existing neuro-monitoring modalities by enabling longitudinal, real-time tracking of cerebrovascular function and recovery trajectories in traumatic brain injury.

Funding

NIH R01 (NIBIB Brain Initiative, 7R01EB031759-03).

Disclosures

The authors declare the following potential conflicts of interest with respect to the research, authorship, and/or publication of this article: U.S and S.S. have a pending patent application relevant to this work.

Code and Data Availability

Data may be provided by the corresponding author upon reasonable request.

Acknowledgements

The authors acknowledge the funding support from NIH R01 (NIBIB Brain Initiative (7R01EB031759-03). We thank Nick Bertone (Picoquant Inc.) for providing the demo unit of HydraHarp400 for the time domain acquisition system. A pre-print version of this manuscript can be found on medRxiv, https://doi.org/10.1101/2025.08.31.25334647. ChatGPT (GPT-4) was used to assist with grammar and language editing during the preparation of this manuscript.

603 **References:**

604

605 1. S. L. James et al., “Global, regional, and national burden of traumatic brain injury and
606 spinal cord injury, 1990-2016: A systematic analysis for the Global Burden of Disease
607 Study 2016,” Lancet Neurol. **18**(1), 56–87, Lancet Publishing Group (2019)
608 [doi:10.1016/S1474-4422(18)30415-0].

609 2. A. L. C. Zaninotto et al., “Traumatic brain injury,” in Clinical Trials in Neurology, F. Fregni,
610 Ed., Humana Press.

611 3. K. Kenney et al., “Cerebral Vascular Injury in Traumatic Brain Injury,” Exp. Neurol. **275**,
612 353–366, Academic Press Inc. (2016) [doi:10.1016/j.expneurol.2015.05.019].

613 4. B. Foreman et al., “Safety and Reliability of Bedside, Single Burr Hole Technique for
614 Intracranial Multimodality Monitoring in Severe Traumatic Brain Injury,” Neurocrit. Care
615 **29**(3), 469–480, Neurocrit Care (2018) [doi:10.1007/S12028-018-0551-7].

616 5. D. K. Sandsmark et al., “Cerebral Microvascular Injury: A Potentially Treatable
617 Endophenotype of Traumatic Brain Injury-Induced Neurodegeneration,” in Neuron **103**(3),
618 pp. 367–379, Cell Press (2019) [doi:10.1016/j.neuron.2019.06.002].

619 6. C. Lazaridis and B. Foreman, “Management Strategies Based on Multi-Modality
620 Neuromonitoring in Severe Traumatic Brain Injury,” Neurotherapeutics **20**(6), 1457–1471,
621 Springer Science and Business Media Deutschland GmbH (2023) [doi:10.1007/S13311-
622 023-01411-2,].

623 7. P. Le Roux et al., “Consensus Summary Statement of the International Multidisciplinary
624 Consensus Conference on Multimodality Monitoring in Neurocritical Care: A statement for
625 healthcare professionals from the Neurocritical Care Society and the European Society of
626 Intensive Care Medicine,” Neurocrit. Care **21**(2), 1–26, Humana Press Inc. (2014)
627 [doi:10.1007/s12028-014-0041-5].

628 8. H. Zhao et al., “Comparison of diffuse correlation spectroscopy analytical models for
629 measuring cerebral blood flow in adults,” J. Biomed. Opt. **28**(12), SPIE-Intl Soc Optical
630 Eng (2023) [doi:10.1117/1.jbo.28.12.126005].

631 9. J. Selb et al., “Sensitivity of near-infrared spectroscopy and diffuse correlation
632 spectroscopy to brain hemodynamics: simulations and experimental findings during
633 hypercapnia,” Neurophotonics **1**(1), 15005, SPIE-Intl Soc Optical Eng (2014)
634 [doi:10.1117/1.nph.1.1.015005].

635 10. L. Qiu et al., “Time Domain Diffuse Correlation Spectroscopy for Detecting Human Brain
636 Function: Optimize System on Real Experimental Conditions by Simulation Method,”
637 IEEE Photonics J. **13**(4), Institute of Electrical and Electronics Engineers Inc. (2021)
638 [doi:10.1109/JPHOT.2021.3089635].

639 11. J. Selb et al., “Prolonged monitoring of cerebral blood flow and autoregulation with diffuse
640 correlation spectroscopy in neurocritical care patients,” Neurophotonics **5**(04), 1, SPIE-
641 Intl Soc Optical Eng (2018) [doi:10.1117/1.NPH.5.4.045005,].

12. D. Mazumder et al., “Optimization of time domain diffuse correlation spectroscopy parameters for measuring brain blood flow,” Neurophotonics **8**(03), SPIE-Intl Soc Optical Eng (2021) [doi:10.1117/1.NPH.8.3.035005,].

13. D. A. Boas et al., “Establishing the diffuse correlation spectroscopy signal relationship with blood flow,” Neurophotonics **3**(3), 31412, SPIE-Intl Soc Optical Eng (2016) [doi:10.1117/1.NPH.3.3.031412,].

14. F. Amyot et al., “A Review of the Effectiveness of Neuroimaging Modalities for the Detection of Traumatic Brain Injury,” J. Neurotrauma **32**(22), 1693–1721, Mary Ann Liebert Inc. (2015) [doi:10.1089/NEU.2013.3306,].

15. X. Cheng et al., “Measuring neuronal activity with diffuse correlation spectroscopy: a theoretical investigation,” Neurophotonics **8**(03), SPIE-Intl Soc Optical Eng (2021) [doi:10.1117/1.NPH.8.3.035004,].

16. J. Li et al., “Characterization of autism spectrum disorder with spontaneous hemodynamic activity,” Biomed. Opt. Express **7**(10), 3871, Optica Publishing Group (2016) [doi:10.1364/BOE.7.003871,].

17. J. Sutin et al., “Time-domain diffuse correlation spectroscopy,” Optica **3**(9), 1006, Optica Publishing Group (2016) [doi:10.1364/OPTICA.3.001006,].

18. O. Kholiqov et al., “Time-of-flight resolved light field fluctuations reveal deep human tissue physiology,” Nature Communications 2020 11:1 **11**(1), 391-, Nature Publishing Group (2020) [doi:10.1038/s41467-019-14228-5].

19. W. Zhou et al., “Multi-exposure interferometric diffusing wave spectroscopy,” Optics Letters, Vol. 46, Issue 18, pp. 4498-4501 **46**(18), 4498–4501, Optica Publishing Group (2021) [doi:10.1364/OL.427746].

20. L. Qiu et al., “Analytical models for time-domain diffuse correlation spectroscopy for multi-layer and heterogeneous turbid media,” Biomedical Optics Express, Vol. 8, Issue 12, pp. 5518-5532 **8**(12), 5518–5532, Optica Publishing Group (2017) [doi:10.1364/BOE.8.005518].

21. L. Qiu et al., “Using a simulation approach to optimize time-domain diffuse correlation spectroscopy measurement on human head,” Neurophotonics **5**(2), 1, Neurophotonics (2018) [doi:10.1117/1.NPH.5.2.025007].

22. T. Ko et al., “Fast blood flow monitoring in deep tissues with real-time software correlators,” Biomedical Optics Express, Vol. 7, Issue 3, pp. 776-797 **7**(3), 776–797, Optica Publishing Group (2016) [doi:10.1364/BOE.7.000776].

23. C.-S. Poon et al., “First-in-clinical application of a time-gated diffuse correlation spectroscopy system at 1064 nm using superconducting nanowire single photon detectors in a neuro intensive care unit,” Biomed. Opt. Express **13**(3), 1344, Optica Publishing Group (2022) [doi:10.1364/boe.448135].

24. M. Pagliazzi et al., “In vivo time domain speckle contrast optical spectroscopy,” in European Conference on Biomedical Optics, Optica Publishing Group.

25. C. S. Poon et al., “Noninvasive optical monitoring of cerebral blood flow and eeg spectral responses after severe traumatic brain injury: A case report,” Brain Sci. **11**(8), MDPI (2021) [doi:10.3390/brainsci11081093].

26. V. Parfentyeva et al., “Fast time-domain diffuse correlation spectroscopy with superconducting nanowire single-photon detector: system validation and in vivo results,” Sci. Rep. **13**(1), Nature Research (2023) [doi:10.1038/s41598-023-39281-5].

27. N. Ozana et al., “Superconducting nanowire single-photon sensing of cerebral blood flow,” Neurophotonics **8**(3), Neurophotonics (2021) [doi:10.1117/1.NPH.8.3.035006].

28. J. Li et al., “Resting-state functional connectivity measured by diffuse correlation spectroscopy,” J. Biophotonics **11**(2), J Biophotonics (2018) [doi:10.1002/JBIO.201700165].

29. D. R. Busch et al., “Continuous cerebral hemodynamic measurement during deep hypothermic circulatory arrest,” Biomed. Opt. Express **7**(9), 3461, Optica Publishing Group (2016) [doi:10.1364/BOE.7.003461,].

30. E. S. Rosenthal et al., “Continuous Electroencephalography Predicts Delayed Cerebral Ischemia after Subarachnoid Hemorrhage: A Prospective Study of Diagnostic Accuracy,” Ann. Neurol. **83**(5), 958, John Wiley and Sons Inc. (2018) [doi:10.1002/ANA.25232].

31. M. Mohtasebi et al., “Detection of low-frequency oscillations in neonatal piglets with speckle contrast diffuse correlation tomography,” J. Biomed. Opt. **28**(12), 121204, SPIE-Intl Soc Optical Eng (2023) [doi:10.1117/1.JBO.28.12.121204].

32. W. B. Baker et al., “Continuous non-invasive optical monitoring of cerebral blood flow and oxidative metabolism after acute brain injury,” Journal of Cerebral Blood Flow and Metabolism **39**(8), 1469–1485, SAGE Publications Ltd (2019) [doi:10.1177/0271678X19846657,].

33. D. J. Davies et al., “Cerebral oxygenation in traumatic brain injury: Can a non-invasive frequency domain near-infrared spectroscopy device detect changes in brain tissue oxygen tension as well as the established invasive monitor?,” J. Neurotrauma **36**(7), 1175–1183, Mary Ann Liebert Inc. (2019) [doi:10.1089/NEU.2018.5667,].

34. C. Du et al., “Low-frequency calcium oscillations accompany deoxyhemoglobin oscillations in rat somatosensory cortex,” Proc. Natl. Acad. Sci. U. S. A. **111**(43), E4677–E4686, National Academy of Sciences (2014) [doi:10.1073/pnas.1410800111].

35. W. Chen et al., “Cocaine Decreases Spontaneous Neuronal Activity and Increases Low-Frequency Neuronal and Hemodynamic Cortical Oscillations,” Cerebral Cortex **29**(4), 1594–1606, Oxford University Press (2019) [doi:10.1093/cercor/bhy057].

36. R. Cheng et al., “Noninvasive optical evaluation of spontaneous low frequency oscillations in cerebral hemodynamics,” Neuroimage **62**(3), 1445–1454 (2012) [doi:10.1016/j.neuroimage.2012.05.069].

37. Y. Li et al., “Systemic low-frequency oscillations observed in the periphery of healthy human subjects,” J. Biomed. Opt. **23**(05), 1, SPIE-Intl Soc Optical Eng (2018) [doi:10.1117/1.JBO.23.5.057001,].

38. G. Bicciato et al., “Increase in Low-Frequency Oscillations in fNIRS as Cerebral Response to Auditory Stimulation with Familiar Music,” Brain Sci. **12**(1), 42, MDPI (2021) [doi:10.3390/BRAINSCI12010042].

39. C. Yaramothu et al., “Reliability of Frontal Eye Fields Activation and Very Low-Frequency Oscillations Observed during Vergence Eye Movements: an fNIRS Study,” Sci. Rep. **10**(1), 1–10, Nature Research (2020) [doi:10.1038/S41598-020-57597-4;TECHMETA=5,59;SUBJMETA=2613,378,3920,631;KWRD=NEURAL+CIRCUITS,VISUAL+SYSTEM].

40. C. Yaramothu et al., “Reliability of Frontal Eye Fields Activation and Very Low-Frequency Oscillations Observed during Vergence Eye Movements: an fNIRS Study,” Scientific Reports 2020 10:1 **10**(1), 712-, Nature Publishing Group (2020) [doi:10.1038/s41598-020-57597-4].

41. A. V. Andersen et al., “Assessing low-frequency oscillations in cerebrovascular diseases and related conditions with near-infrared spectroscopy: a plausible method for evaluating cerebral autoregulation?,” Neurophotonics **5**(3), 30901, SPIE-Intl Soc Optical Eng (2018) [doi:10.1117/1.NPH.5.3.030901].

42. Y. Tong et al., “Low-frequency oscillations measured in the periphery with near-infrared spectroscopy are strongly correlated with blood oxygen level-dependent functional magnetic resonance imaging signals,” J. Biomed. Opt. **17**(10), 1, SPIE-Intl Soc Optical Eng (2012) [doi:10.1117/1.JBO.17.10.106004,].

43. V. Chernomordik et al., “Abnormality of low frequency cerebral hemodynamics oscillations in TBI population,” Brain Res. **1639**, 194–199, Elsevier B.V. (2016) [doi:10.1016/j.brainres.2016.02.018].

44. M. Y. Wang et al., “Functional near-infrared spectroscopy can detect low-frequency hemodynamic oscillations in the prefrontal cortex during steady-state visual evoked potential-inducing periodic facial expression stimuli presentation,” Vis. Comput. Ind. Biomed. Art **3**(1), 1–8, Springer Science and Business Media B.V. (2020) [doi:10.1186/S42492-020-00065-7/FIGURES/8].

45. S. Schulthess et al., “Low frequency oscillations reflect neurovascular coupling and disappear after cerebral death,” Scientific Reports 2024 14:1 **14**(1), 1–10, Nature Publishing Group (2024) [doi:10.1038/s41598-024-61819-4].

46. D. Phillip et al., “Low frequency oscillations in cephalic vessels assessed by near infrared spectroscopy,” Eur. J. Clin. Invest. **42**(11), 1180–1188, Eur J Clin Invest (2012) [doi:10.1111/J.1365-2362.2012.02704.X,].

47. H. Obrig et al., “Spontaneous low frequency oscillations of cerebral hemodynamics and metabolism in human adults,” Neuroimage **12**(6), 623–639, Academic Press Inc. (2000) [doi:10.1006/nimg.2000.0657].

48. C. Yeo et al., “Low frequency oscillations assessed by diffuse speckle contrast analysis for foot angiosome concept,” Scientific Reports 2020 10:1 **10**(1), 1–14, Nature Publishing Group (2020) [doi:10.1038/s41598-020-73604-0].

49. Y. Tong, L. M. Hocke, and B. B. Frederick, “Low Frequency Systemic Hemodynamic ‘Noise’ in Resting State BOLD fMRI: Characteristics, Causes, Implications, Mitigation Strategies, and Applications,” Front. Neurosci. **13**(JUL), 787, Frontiers Media S.A. (2019) [doi:10.3389/FNINS.2019.00787].

50. A. Vermeij et al., “Very-low-frequency oscillations of cerebral hemodynamics and blood pressure are affected by aging and cognitive load,” Neuroimage **85**, 608–615, Neuroimage (2014) [doi:10.1016/j.neuroimage.2013.04.107].

51. B. R. White et al., “Low frequency power in cerebral blood flow is a biomarker of neurologic injury in the acute period after cardiac arrest,” Resuscitation **178**, 12–18, Elsevier Ireland Ltd (2022) [doi:10.1016/j.resuscitation.2022.07.004].

52. M. J. Lowe, B. J. Mock, and J. A. Sorenson, “Functional Connectivity in Single and Multislice Echoplanar Imaging Using Resting-State Fluctuations,” Neuroimage **7**(2), 119–132, Academic Press (1998) [doi:10.1006/NIMG.1997.0315].

53. N. Lodha and E. A. Christou, “Low-Frequency Oscillations and Control of the Motor Output,” Front. Physiol. **8**(FEB), 78, Frontiers Research Foundation (2017) [doi:10.3389/FPHYS.2017.00078].

54. J. Selb et al., “Prolonged monitoring of cerebral blood flow and autoregulation with diffuse correlation spectroscopy in neurocritical care patients,” Neurophotonics **5**(04), 1, SPIE-Intl Soc Optical Eng (2018) [doi:10.1117/1.NPH.5.4.045005,].

55. W. B. Baker et al., “Continuous non-invasive optical monitoring of cerebral blood flow and oxidative metabolism after acute brain injury,” Journal of Cerebral Blood Flow and Metabolism **39**(8), 1469–1485, SAGE Publications Ltd (2019) [doi:10.1177/0271678X19846657,].

56. D. R. Busch et al., “Detection of Brain Hypoxia Based on Noninvasive Optical Monitoring of Cerebral Blood Flow with Diffuse Correlation Spectroscopy,” Neurocrit. Care **30**(1), 72–80, Humana Press Inc. (2019) [doi:10.1007/S12028-018-0573-1,].

57. R. M. Forti et al., “Transcranial Optical Monitoring of Cerebral Hemodynamics in Acute Stroke Patients during Mechanical Thrombectomy,” Journal of Stroke and Cerebrovascular Diseases **28**(6), 1483–1494, W.B. Saunders (2019) [doi:10.1016/J.JSTROKECEREBROVASDIS.2019.03.019].

58. T. Durduran and A. G. Yodh, “Diffuse correlation spectroscopy for non-invasive, micro-vascular cerebral blood flow measurement,” Neuroimage **85**(0 1), 51, Academic Press Inc. (2014) [doi:10.1016/j.neuroimage.2013.06.017].

59. M. N. Kim et al., “Continuous optical monitoring of cerebral hemodynamics during head-of-bed manipulation in brain-injured adults,” Neurocrit. Care **20**(3), 443–453, Humana Press Inc. (2014) [doi:10.1007/S12028-013-9849-7/FIGURES/2].

60. C. G. Favilla et al., “Optical bedside monitoring of cerebral blood flow in acute ischemic stroke patients during head-of-bed manipulation,” Stroke **45**(5), 1269–1274, Lippincott Williams and Wilkins (2014) [doi:10.1161/STROKEAHA.113.004116/-/DC1].

61. E. M. Buckley et al., “Diffuse correlation spectroscopy for measurement of cerebral blood flow: future prospects,” Neurophotonics **1**(1), 11009, SPIE-Intl Soc Optical Eng (2014) [doi:10.1117/1.NPh.1.1.011009].

62. H. L et al., “Noninvasive continuous optical monitoring of absolute cerebral blood flow in critically ill adults,” Neurophotonics **5**(4), 1, Neurophotonics (2018) [doi:10.1117/1.NPH.5.4.045006].

63. M. Diop et al., “Development of a combined broadband near-infrared and diffusion correlation system for monitoring cerebral blood flow and oxidative metabolism in preterm infants,” Biomed. Opt. Express **6**(10) (2015) [doi:10.1364/boe.6.003907].

64. K. Verdecchia et al., “Quantifying the cerebral metabolic rate of oxygen by combining diffuse correlation spectroscopy and time-resolved near-infrared spectroscopy,” J. Biomed. Opt. (2013) [doi:10.1117/1.jbo.18.2.027007].

65. M. Suwalski et al., “The Effect of Hypotension on Cerebral Metabolism and Perfusion in Adults Undergoing Cardiopulmonary Bypass: A Prospective Cohort Study,” Anesth. Analg. **141**(5), Anesth Analg (2025) [doi:10.1213/ANE.0000000000007607].

66. A. Demertzi et al., “Intrinsic functional connectivity differentiates minimally conscious from unresponsive patients,” Brain **138**(Pt 9), 2619–2631, Brain (2015) [doi:10.1093/BRAIN/AWV169].

67. J. T. Giacino et al., “The minimally conscious state: Definition and diagnostic criteria,” Neurology **58**(3) (2002) [doi:10.1212/WNL.58.3.349].

68. G. B. Narula et al., “Functional NIRS to detect covert consciousness in neurocritical patients,” Clin. Neurophysiol **144**, 72–82.

69. M. M. Monti et al., “Willful Modulation of Brain Activity in Disorders of Consciousness,” New England Journal of Medicine **362**(7), 579–589, Massachusetts Medical Society (2010) [doi:10.1056/NEJMOA0905370;WGROUP:STRING:MMS].

70. C. C. H. Lo, P. Y. M. Woo, and V. C. K. Cheung, “Task-based EEG and fMRI paradigms in a multimodal clinical diagnostic framework for disorders of consciousness,” Rev. Neurosci. **35**(7), 775–787, Rev Neurosci (2024) [doi:10.1515/REVNEURO-2023-0159].

71. E. M. Buckley et al., “Diffuse correlation spectroscopy for measurement of cerebral blood flow: future prospects,” https://doi.org/10.1117/1.NPh.1.1.011009 **1**(1), 11009, SPIE (2014) [doi:10.1117/1.NPH.1.1.011009].

72. L. Cortese et al., “Recipes for diffuse correlation spectroscopy instrument design using commonly utilized hardware based on targets for signal-to-noise ratio and precision,” Biomedical Optics Express, Vol. 12, Issue 6, pp. 3265-3281 **12**(6), 3265–3281, Optica Publishing Group (2021) [doi:10.1364/BOE.423071].

73. D. R. Busch et al., “Laser safety in fiber-optic monitoring of spinal cord hemodynamics: a preclinical evaluation,” J. Biomed. Opt. (2018) [doi:10.1117/1.jbo.23.6.065003].

74. L. Qiu et al., “Using a simulation approach to optimize time-domain diffuse correlation spectroscopy measurement on human head,” Neurophotonics **5**(02), 1 (2018) [doi:10.1117/1.nph.5.2.025007].

75. J. Li et al., “Analytical models for time-domain diffuse correlation spectroscopy for multi-layer and heterogeneous turbid media,” Biomed. Opt. Express **8**(12), 5518, Optica Publishing Group (2017) [doi:10.1364/BOE.8.005518,].

76. S. A. Carp et al., “Diffuse correlation spectroscopy measurements of blood flow using 1064 nm light,” J. Biomed. Opt. **25**(9), J Biomed Opt (2020) [doi:10.1117/1.JBO.25.9.097003].

77. L. Colombo et al., “In vivo time-domain diffuse correlation spectroscopy above the water absorption peak,” Opt. Lett. **45**(13), 3377, Optica Publishing Group (2020) [doi:10.1364/ol.392355].

78. S. Sabaghian et al., “Depth-sensitive assessment of cerebral blood flow and low-frequency oscillations after traumatic brain injury in mice using time-domain diffuse correlation spectroscopy,” Neurophotonics **13**(01) (2026) [doi:10.1117/1.NPh.13.1.015003].

79. M. M. Monti et al., “Willful modulation of brain activity in disorders of consciousness,” N. Engl. J. Med. **362**(7), 579–589, N Engl J Med (2010) [doi:10.1056/NEJMOA0905370].

80. K. Kazazian et al., “Functional near-infrared spectroscopy: A novel tool for detecting consciousness after acute severe brain injury,” Proceedings of the National Academy of Sciences **121**(36), e2402723121, National Academy of Sciences (2024) [doi:10.1073/PNAS.2402723121].

81. S. Schulthess et al., “Low frequency oscillations reflect neurovascular coupling and disappear after cerebral death,” Scientific Reports 2024 14:1 **14**(1), 1–10, Nature Publishing Group (2024) [doi:10.1038/s41598-024-61819-4].

82. T. Durduran and A. G. Yodh, “Diffuse correlation spectroscopy for non-invasive, micro-vascular cerebral blood flow measurement,” Neuroimage **85**(0 1), 51, Academic Press Inc. (2014) [doi:10.1016/j.neuroimage.2013.06.017].

83. D. A. Boas and A. G. Yodh, “Spatially varying dynamical properties of turbid media probed with diffusing temporal light correlation,” Journal of The Optical Society of America A-optics Image Science and Vision **14**(1), 192, Optica Publishing Group (1997) [doi:10.1364/JOSAA.14.000192].

84. D. A. Boas, L. E. Campbell, and A. G. Yodh, “Scattering and imaging with diffusing temporal field correlations,” Phys. Rev. Lett. **75**(9), 1855–1858, Phys Rev Lett (1995) [doi:10.1103/PHYSREVLETT.75.1855,].

85. R. C. Mesquita et al., “Direct measurement of tissue blood flow and metabolism with diffuse optics,” Philosophical Transactions of the Royal Society A: Mathematical, Physical and Engineering Sciences **369**(1955), 4390–4406, The Royal Society Publishing (2011) [doi:10.1098/RSTA.2011.0232].

86. M. N. Kim et al., “Continuous optical monitoring of cerebral hemodynamics during head-of-bed manipulation in brain-injured adults,” Neurocrit. Care **20**(3), 443–453, Humana Press Inc. (2014) [doi:10.1007/S12028-013-9849-7/FIGURES/2].

87. D. Tamborini et al., “Portable System for Time-Domain Diffuse Correlation Spectroscopy,” IEEE Trans. Biomed. Eng. **66**(11), 3014–3025, IEEE Computer Society (2019) [doi:10.1109/TBME.2019.2899762].

88. R. Erdmann et al., “Time domain diffuse correlation spectroscopy with a high coherence pulsed source: in vivo and phantom results,” Biomedical Optics Express, Vol. 8, Issue 11, pp. 5311-5325 **8**(11), 5311–5325, Optica Publishing Group (2017) [doi:10.1364/BOE.8.005311].

89. L. Shi et al., “Transmission in near-infrared optical windows for deep brain imaging,” J. Biophotonics **9**(1–2), 38–43, Wiley-VCH Verlag (2016) [doi:10.1002/JBIO.201500192;PAGEGROUP:STRING:PUBLICATION].

90. L. A. Sordillo et al., “Deep optical imaging of tissue using the second and third near-infrared spectral windows,” https://doi.org/10.1117/1.JBO.19.5.056004 **19**(5), 56004, SPIE (2014) [doi:10.1117/1.JBO.19.5.056004].

91. W. Liu et al., “Fast and sensitive diffuse correlation spectroscopy with highly parallelized single photon detection,” APL Photonics **6**(2), 26106, American Institute of Physics Inc. (2021) [doi:10.1063/5.0031225/1062592].

92. M. Azimipour et al., “Fluorescence laminar optical tomography for brain imaging: system implementation and performance evaluation,” J Biomed Opt **22**(1), 2017/01/06, 16003 (2017) [doi:10.1117/1.JBO.22.1.016003].

93. C. Poon et al., “Cerebral blood flow-based resting state functional connectivity of the human brain using optical diffuse correlation spectroscopy,” Journal of Visualized Experiments **2020**(159), 1–7, Journal of Visualized Experiments (2020) [doi:10.3791/60765,].

94. A. Pifferi et al., “Time-resolved diffuse reflectance using small source-detector separation and fast single-photon gating,” Phys. Rev. Lett. **100**(13), Phys Rev Lett (2008) [doi:10.1103/PHYSREVLETT.100.138101,].

95. L. Colombo et al., “Effects of the instrument response function and the gate width in time-domain diffuse correlation spectroscopy: model and validations,” https://doi.org/10.1117/1.NPh.6.3.035001 **6**(3), 35001, SPIE (2019) [doi:10.1117/1.NPH.6.3.035001].

96. S. Samaei et al., “Time-domain diffuse correlation spectroscopy (TD-DCS) for noninvasive, depth-dependent blood flow quantification in human tissue in vivo,” Sci. Rep. **11**(1), Nature Research (2021) [doi:10.1038/s41598-021-81448-5].

97. S. Tagliabue et al., “How the heterogeneity of the severely injured brain affects hybrid diffuse optical signals: case examples and guidelines,” Neurophotonics **11**(4), Neurophotonics (2024) [doi:10.1117/1.NPH.11.4.045005].

98. B. C. Wilson, B. Chance, and M. S. Patterson, “Time resolved reflectance and transmittance for the noninvasive measurement of tissue optical properties,” Applied Optics, Vol. 28, Issue 12, pp. 2331-2336 **28**(12), 2331–2336, Optica Publishing Group (1989) [doi:10.1364/ao.28.002331].

99. F. Martelli, D. Contini, and G. Zaccanti, “Photon migration through a turbid slab described by a model based on diffusion approximation. I. Theory,” Applied Optics, Vol. 36, Issue 19, pp. 4587-4599 **36**(19), 4587–4599, Optica Publishing Group (1997) [doi:10.1364/ao.36.004587].

100. J. Li et al., “Analytical models for time-domain diffuse correlation spectroscopy for multi-layer and heterogeneous turbid media,” Biomed. Opt. Express **8**(12), 5518, Optica Publishing Group (2017) [doi:10.1364/BOE.8.005518,].

101. S. R. Gohel and B. B. Biswal, “Functional integration between brain regions at rest occurs in multiple-frequency bands,” Brain Connect. **5**(1) (2015) [doi:10.1089/brain.2013.0210].

102. D. J. Hodkinson et al., “Increased amplitude of thalamocortical low-frequency oscillations in patients with migraine,” Journal of Neuroscience **36**(30) (2016) [doi:10.1523/JNEUROSCI.1038-16.2016].

103. C. La et al., “Differing patterns of altered slow-5 oscillations in healthy aging and ischemic stroke,” Front. Hum. Neurosci. **10**(APR2016), 1–14, Frontiers Media S. A (2016) [doi:10.3389/FNHUM.2016.00156,].

104. H. Cheng et al., “Power spectrum of spontaneous cerebral homodynamic oscillation shows a distinct pattern in autism spectrum disorder,” Biomed. Opt. Express **10**, 1383–1392.

105. W. Chen et al., “Interactions between stimuli-evoked cortical activity and spontaneous low frequency oscillations measured with neuronal calcium,” Neuroimage **210**, Academic Press Inc. (2020) [doi:10.1016/J.NEUROIMAGE.2020.116554,].

106. D. S. Langri and U. Sunar, “Non-Invasive Continuous Optical Monitoring of Cerebral Blood Flow after Traumatic Brain Injury in Mice Using Fiber Camera-Based Speckle Contrast Optical Spectroscopy,” Brain Sci. **13**(10), Multidisciplinary Digital Publishing Institute (MDPI) (2023) [doi:10.3390/BRAINSCI13101365,].

107. A. Fanta et al., “Assessment of cerebral autoregulation and cerebral perfusion in patients with sickle cell disease using frequency-domain near-infrared spectroscopy,” J. Appl. Physiol. **139**(3), 638–649, American Physiological Society (2025) [doi:10.1152/JAPPLPHYSIOL.00426.2023].

108. N. F. Chi et al., “Dynamic Cerebral Autoregulation Is an Independent Functional Outcome Predictor of Mild Acute Ischemic Stroke,” Stroke **49**(11), 2605–2611, Stroke (2018) [doi:10.1161/STROKEAHA.118.022481].

109. H. Cheng et al., “Power spectrum of spontaneous cerebral homodynamic oscillation shows a distinct pattern in autism spectrum disorder,” Biomed. Opt. Express **10**(3), 1383, Biomed Opt Express (2019) [doi:10.1364/BOE.10.001383].

110. S. Wood et al., “Assessing Dynamic Cerebral Autoregulation in Patients with Sickle Cell Disease Using Near-Infrared Spectroscopy and Paced Breathing,” Blood **136**(Supplement 1), 57–58, American Society of Hematology (2020) [doi:10.1182/BLOOD-2020-137624].

111. Y. Tong and B. Frederick, “Concurrent fNIRS and fMRI processing allows independent visualization of the propagation of pressure waves and bulk blood flow in the cerebral vasculature,” Neuroimage **61**, 1419–1427.

112. L. Duan, Y. J. Zhang, and C. Z. Zhu, “Quantitative comparison of resting-state functional connectivity derived from fNIRS and fMRI: A simultaneous recording study,” Neuroimage **60**, 2008–2018.

113. L. Gagnon et al., “Further improvement in reducing superficial contamination in NIRS using double short separation measurements,” Neuroimage **85**(0 1), 127–135, Neuroimage (2014) [doi:10.1016/j.neuroimage.2013.01.073].

114. S. Särkkä et al., “Dynamic retrospective filtering of physiological noise in BOLD fMRI: DRIFTER,” Neuroimage **60**(2) (2012) [doi:10.1016/j.neuroimage.2012.01.067].

115. E. Kirilina et al., “The physiological origin of task-evoked systemic artefacts in functional near infrared spectroscopy,” Neuroimage **61**(1), 70–81, Academic Press (2012) [doi:10.1016/j.neuroimage.2012.02.074].

116. L. Gagnon et al., “Further improvement in reducing superficial contamination in NIRS using double short separation measurements,” Neuroimage **85**(0 1), 127–135, Neuroimage (2014) [doi:10.1016/j.neuroimage.2013.01.073].

117. T. J. Huppert et al., “A temporal comparison of BOLD, ASL, and NIRS hemodynamic responses to motor stimuli in adult humans,” Neuroimage **29**(2), 368–382, Academic Press (2006) [doi:10.1016/j.neuroimage.2005.08.065].

118. L. Gagnon et al., “Quantification of the cortical contribution to the NIRS signal over the motor cortex using concurrent NIRS-fMRI measurements,” Neuroimage **59**(4), 3933–3940, Neuroimage (2012) [doi:10.1016/j.neuroimage.2011.10.054].

119. G. R. Wu et al., “Modulation of the spontaneous hemodynamic response function across levels of consciousness,” Neuroimage **200**, 450–459, Academic Press Inc. (2019) [doi:10.1016/j.neuroimage.2019.07.011].

120. H. Lu et al., “A functional near-infrared spectroscopy study on hemodynamic changes of patients with prolonged disorders of consciousness responding to different auditory stimuli,” BMC Neurology 2023 23:1 **23**(1), 242-, BioMed Central (2023) [doi:10.1186/S12883-023-03292-6].

121. M. Li et al., “Detecting Residual Awareness in Patients With Prolonged Disorders of Consciousness: An fNIRS Study,” Front. Neurol. **12**, Front Neurol (2021) [doi:10.3389/FNEUR.2021.618055].

122. G. Bicciato et al., “Functional NIRS to detect covert consciousness in neurocritical patients,” Clinical Neurophysiology **144**, 72–82, Elsevier Ireland Ltd (2022) [doi:10.1016/j.clinph.2022.10.002].

123. A. M. Owen et al., “Detecting awareness in the vegetative state,” Science **313**(5792), 1402, Science (2006) [doi:10.1126/SCIENCE.1130197].

124. M. Boly et al., “Functional connectivity in the default network during resting state is preserved in a vegetative but not in a brain dead patient,” Hum. Brain Mapp. **30**(8), 2393 (2009) [doi:10.1002/HBM.20672].

125. J. Stender et al., “Diagnostic precision of PET imaging and functional MRI in disorders of consciousness: A clinical validation study,” The Lancet **384**(9942), 514–522, Elsevier B.V. (2014) [doi:10.1016/S0140-6736(14)60042-8].

126. B. Hermann et al., “Multimodal FDG-PET and EEG assessment improves diagnosis and prognostication of disorders of consciousness,” Neuroimage Clin. **30**, 102601, Elsevier (2021) [doi:10.1016/J.NICL.2021.102601].

127. J. T. Giacino et al., “Comprehensive systematic review update summary: Disorders of consciousness: Report of the Guideline Development, Dissemination, and Implementation Subcommittee of the American Academy of Neurology; the American Congress of Rehabilitation Medicine; and th…,” Neurology **91**(10), 461, Lippincott Williams and Wilkins (2018) [doi:10.1212/WNL.0000000000005928].

128. F. Dondi et al., “The Role of [18F]FDG PET Imaging for the Assessment of Vegetative State or Unresponsive Wakefulness Syndrome: A Systematic Review,” Diagnostics **15**(11), 1406, Multidisciplinary Digital Publishing Institute (MDPI) (2025) [doi:10.3390/DIAGNOSTICS15111406/S1].

129. C. C. H. Lo, P. Y. M. Woo, and V. C. K. Cheung, “Task-based EEG and fMRI paradigms in a multimodal clinical diagnostic framework for disorders of consciousness,” Rev. Neurosci. **35**(7), 775–787, Rev Neurosci (2024) [doi:10.1515/REVNEURO-2023-0159].

130. H. Huang et al., “Early Consciousness Disorder in Acute Large Hemispheric Infarction: An Analysis Based on Quantitative EEG and Brain Network Characteristics,” Neurocrit. Care **33**(2), 376–388, Springer (2020) [doi:10.1007/s12028-020-01051-w].

131. J. Claassen et al., “Detection of Brain Activation in Unresponsive Patients with Acute Brain Injury,” N. Engl. J. Med. **380**(26), 2497–2505, N Engl J Med (2019) [doi:10.1056/NEJMOA1812757].

132. J. Claassen et al., “Detection of Brain Activation in Unresponsive Patients with Acute Brain Injury,” New England Journal of Medicine **380**(26), 2497–2505, Massachusetts Medical Society (2019) [doi:10.1056/NEJMOA1812757;WGROUP:STRING:MMS].

133. P. Le Roux et al., “Consensus Summary Statement of the International Multidisciplinary Consensus Conference on Multimodality Monitoring in Neurocritical Care: A statement for healthcare professionals from the Neurocritical Care Society and the European Society of Intensive Care Medicine,” Neurocrit. Care **21**(2), 1–26, Humana Press Inc. (2014) [doi:10.1007/s12028-014-0041-5].

134. M. H. Othman et al., “Resting-State NIRS–EEG in Unresponsive Patients with Acute Brain Injury: A Proof-of-Concept Study,” Neurocrit. Care **34**(1) (2021) [doi:10.1007/s12028-020-00971-x].

135. G. Bicciato et al., “Functional NIRS to detect covert consciousness in neurocritical patients,” Clinical Neurophysiology **144**, 72–82 (2022) [doi:https://doi.org/10.1016/j.clinph.2022.10.002].

136. L. Bastian et al., “Sensitive and specific fNIRS-based approach for awareness detection in disorders of consciousness: proof of principle in healthy adults,” Neurophotonics **12**(4), Neurophotonics (2025) [doi:10.1117/1.NPH.12.4.045001].

137. Y. Bai, Y. Lin, and U. Ziemann, “Managing disorders of consciousness: the role of electroencephalography,” J. Neurol. **268**(11), 4033, Springer Science and Business Media Deutschland GmbH (2020) [doi:10.1007/S00415-020-10095-Z].

138. J. D. Sitt et al., “Large scale screening of neural signatures of consciousness in patients in a vegetative or minimally conscious state,” Brain **137**(8), 2258–2270, Oxford Academic (2014) [doi:10.1093/BRAIN/AWU141].

139. E. Kirilina et al., “The physiological origin of task-evoked systemic artefacts in functional near infrared spectroscopy,” Neuroimage **61**(1), 70–81, Academic Press (2012) [doi:10.1016/J.NEUROIMAGE.2012.02.074].

140. U. Chaudhary et al., “Brain–Computer Interface–Based Communication in the Completely Locked-In State,” PLoS Biol. **15**(1), e1002593, Public Library of Science (2017) [doi:10.1371/JOURNAL.PBIO.1002593].

141. Y. Wang et al., “Detecting cognitive motor dissociation by functional near-infrared spectroscopy,” Front. Neurol. **16**, 1532804, Frontiers Media SA (2025) [doi:10.3389/FNEUR.2025.1532804/FULL].

142. L. Colombo et al., “In vivo time-domain diffuse correlation spectroscopy above the water absorption peak,” Opt. Lett. **45**(13), 3377, Optica Publishing Group (2020) [doi:10.1364/ol.392355].

143. S. Schulthess et al., “Low frequency oscillations reflect neurovascular coupling and disappear after cerebral death,” Scientific Reports 2024 14:1 **14**(1), 1–10, Nature Publishing Group (2024) [doi:10.1038/s41598-024-61819-4].

144. V. Chernomordik et al., “Abnormality of low frequency cerebral hemodynamics oscillations in TBI population,” Brain Res. **1639**, 194–199, Elsevier B.V. (2016) [doi:10.1016/j.brainres.2016.02.018].

145. A. V. Andersen et al., “Assessing low-frequency oscillations in cerebrovascular diseases and related conditions with near-infrared spectroscopy: a plausible method for evaluating cerebral autoregulation?,” Neurophotonics **5**(3), 30901, SPIE-Intl Soc Optical Eng (2018) [doi:10.1117/1.NPH.5.3.030901].

146. B. R. White et al., “Low frequency power in cerebral blood flow is a biomarker of neurologic injury in the acute period after cardiac arrest,” Resuscitation **178**, 12–18, Elsevier Ireland Ltd (2022) [doi:10.1016/j.resuscitation.2022.07.004].

147. C. Zweifel et al., “Continuous monitoring of cerebrovascular pressure reactivity in patients with head injury,” Neurosurg. Focus **25**(4), Neurosurg Focus (2008) [doi:10.3171/FOC.2008.25.10.E2].

148. A. Sassaroli et al., “Low-frequency spontaneous oscillations of cerebral hemodynamics investigated with near-infrared spectroscopy: A review,” in IEEE Journal on Selected Topics in Quantum Electronics **18**(4) (2012) [doi:10.1109/JSTQE.2012.2183581].

149. G. R. Wu et al., “Modulation of the spontaneous hemodynamic response function across levels of consciousness,” Neuroimage **200**, 450–459, Academic Press Inc. (2019) [doi:10.1016/j.neuroimage.2019.07.011].

150. A. Farina et al., “In-vivo multilaboratory investigation of the optical properties of the human head,” Biomed. Opt. Express **6**(7), 2609, Optica Publishing Group (2015) [doi:10.1364/boe.6.002609].

151. G. Giacalone et al., “Cerebral time domain-NIRS: reproducibility analysis, optical properties, hemoglobin species and tissue oxygen saturation in a cohort of adult subjects,” Biomed. Opt. Express **8**(11), 4987, Optica Publishing Group (2017) [doi:10.1364/boe.8.004987].

152. J. M. Kainerstorfer et al., “Cerebral autoregulation in the microvasculature measured with near-infrared spectroscopy,” J. Cereb. Blood Flow Metab. **35**(6), 959–966, J Cereb Blood Flow Metab (2015) [doi:10.1038/JCBFM.2015.5].

153. D. Phillip et al., “Spontaneous Low Frequency Oscillations in Acute Ischemic Stroke – A Near Infrared Spectroscopy (NIRS) Study” (2014) [doi:10.4172/2155-9562.1000241].

154. A. Fanta et al., “Assessment of cerebral autoregulation and cerebral perfusion in patients with sickle cell disease using frequency-domain near-infrared spectroscopy,” J. Appl. Physiol. (1985). **139**(3), 638–649, J Appl Physiol (1985) (2025) [doi:10.1152/JAPPLPHYSIOL.00426.2023].

155. R. C. Nogueira et al., “Review of studies on dynamic cerebral autoregulation in the acute phase of stroke and the relationship with clinical outcome,” J. Cereb. Blood Flow Metab. **42**(3), 430–453, J Cereb Blood Flow Metab (2022) [doi:10.1177/0271678X211045222].

156. H. Cheng et al., “Power spectrum of spontaneous cerebral homodynamic oscillation shows a distinct pattern in autism spectrum disorder,” Biomed. Opt. Express **10**, 1383–1392.

157. C. M. Lu et al., “Use of fNIRS to assess resting state functional connectivity,” J. Neurosci. Methods **186**, 242–249.

158. R. F. Rojas et al., “Physiological fluctuations show frequency-specific networks in fNIRS signals during resting state,” in Proceedings of the 39th Annual International Conference of the IEEE Engineering in Medicine and Biology Society, Jeju, Republic of Korea.

159. B. Foreman and J. Claassen, “Quantitative EEG for the detection of brain ischemia,” Crit. Care **16**(2), Crit Care (2012) [doi:10.1186/CC11230,].

1112

1113

1114

1115 **Supplementary Table S1.** Clinical characteristics and experimental inclusion of all subjects.

Subject	Diagnosis	Age	Sex	Hemorrhage	Surgery	Resting-State (Fig. 3)	Smile Task (Fig. 4)	Notes
H1–H25	Healthy	21–39 (mean 26.9 ± 4.8)	14 M / 11 F	No	No	Yes	No	Resting-state cohort
H26–H30	Healthy	25–35 (mean 29.0 ± 5.5)	5 M	No	No	No	Yes	Smile-task cohort
MCS-1	MCS	40	M	No	No	Yes	Yes	Resting-state only
MCS-2	MCS	75	M	Yes (left temporal)	No	Yes	No	Resting-state only
UWS-1	UWS	40	M	Yes (multicompartmental)	Yes (decompressive craniectomy + skull reattachment)	No	Yes	Dual-probe bilateral + task
Coma-1	Coma	40	M	No	No	Yes	No	Resting-state only
Coma-2	Coma	40	M	No	No	Yes	No	Resting-state only
Coma-3	Coma	70	M	No	No	Yes	No	Resting-state only